

Research Articles: Development/Plasticity/Repair**Complement C5aR1 Signaling Promotes Polarization and Proliferation of Embryonic Neural Progenitor Cells through PKC#.**

Liam G. Coulthard^{1,a,b}, Owen A. Hawsworth^{1,c,d}, Rui Li^c, Anushree Balachandran^d, John D. Lee^c, Farshid Sepehrband^{a,f}, Nyoman Kurniawan^e, Angela Jeanes^c, David G. Simmons^c, Ernst Woltetang^d and Trent M. Woodruff^c

^aRoyal Brisbane and Women's Hospital, Herston, QLD, Australia

^bSchool of Medicine, The University of Queensland, Herston, QLD, Australia

^cSchool of Biomedical Sciences, The University of Queensland, St Lucia, QLD, Australia

^dAustralian Institute for Bioengineering and Nanotechnology, The University of Queensland, St Lucia, QLD, Australia

^eCentre for Advanced Imaging, The University of Queensland, St Lucia, QLD, Australia

^fLaboratory of Neuro Imaging, USC Mark and Mary Stevens Neuroimaging and Informatics Institute, Keck School of Medicine, University of Southern California, Los Angeles, CA, USA.

DOI: 10.1523/JNEUROSCI.0525-17.2017

Received: 22 February 2017

Revised: 3 April 2017

Accepted: 13 April 2017

Published: 28 April 2017

Author contributions: L.G.C., O.A.H., F.S., N.K., D.G.S., E.W., and T.M.W. designed research; L.G.C., O.A.H., R.L., A.B., and J.D.L. performed research; L.G.C., O.A.H., R.L., F.S., N.K., A.J., and T.M.W. analyzed data; L.G.C., O.A.H., A.J., D.G.S., E.W., and T.M.W. wrote the paper.

Conflict of Interest: Competing interests: The authors declare no competing financial interests.

¹These authors contributed equally.

We acknowledge support from an ARC Centre of Excellence "Stem Cells Australia" (SR110001002, E.W.) and a National Health and Medical Research Council (NHMRC) Project grant (APP1082271, TMW). TMW is supported by a NHMRC Career Development Fellowship (APP1105420).

Correspondence: Associate Professor Trent M. Woodruff, School of Biomedical Sciences, The University of Queensland, St Lucia, Brisbane, QLD, 4072, AUSTRALIA, t.woodruff@uq.edu.au, Ph: +61 7 3365 2924, Fax: +61 7 3365 1766; Professor Ernst Woltetang, Australian Institute for Bioengineering & Nanotechnology, The University of Queensland, St Lucia, Brisbane, QLD, 4072, AUSTRALIA, e.woltetang@uq.edu.au, Ph: +61 7 3346 3894, Fax: +61 7 3346 3973

Cite as: J. Neurosci ; 10.1523/JNEUROSCI.0525-17.2017

Alerts: Sign up at www.jneurosci.org/cgi/alerts to receive customized email alerts when the fully formatted version of this article is published.

Accepted manuscripts are peer-reviewed but have not been through the copyediting, formatting, or proofreading process.

1 **Complement C5aR1 Signaling Promotes Polarization and Proliferation of**
2 **Embryonic Neural Progenitor Cells through PKC ζ .**

3 Abbreviated Title: C5aR1 Drives Neural Progenitor Proliferation.

4 Liam G. Coulthard^{a,b,1}, Owen A. Hawksworth^{c,d,1}, Rui Li^c, Anushree Balachandran^d, John D. Lee^c,
5 Farshid Sepehrband^{e,f}, Nyoman Kurniawan^e, Angela Jeanes^c, David G. Simmons^c, Ernst
6 Wolvetang^{d,2} & Trent M. Woodruff^{c,2}

7 ^aRoyal Brisbane and Women's Hospital, Herston, QLD, Australia

8 ^bSchool of Medicine, The University of Queensland, Herston, QLD, Australia

9 ^cSchool of Biomedical Sciences, The University of Queensland, St Lucia, QLD, Australia

10 ^dAustralian Institute for Bioengineering and Nanotechnology, The University of Queensland, St Lucia, QLD, Australia

11 ^eCentre for Advanced Imaging, The University of Queensland, St Lucia, QLD, Australia

12 ^fLaboratory of Neuro Imaging, USC Mark and Mary Stevens Neuroimaging and Informatics Institute, Keck School of Medicine,
13 University of Southern California, Los Angeles, CA, USA.

14 ¹These authors contributed equally. ²Corresponding authors.

15

16 Correspondence:

17 Associate Professor Trent M. Woodruff
18 School of Biomedical Sciences
19 The University of Queensland
20 St Lucia, Brisbane, QLD, 4072
21 AUSTRALIA
22 t.woodruff@uq.edu.au
23 Ph: +61 7 3365 2924
24 Fax: +61 7 3365 1766

Professor Ernst Wolvetang
Australian Institute for Bioengineering &
Nanotechnology
The University of Queensland
St Lucia, Brisbane, QLD, 4072
AUSTRALIA
e.wolvetang@uq.edu.au
Ph: +61 7 3346 3894
Fax: +61 7 3346 3973

26 **Manuscript Details**

27 Pages: 40

28 Figures: 6

29 Tables: 2

30 Word count: Abstract 249; Introduction 466; Materials & Methods 2487; Results 2051; Discussion 1263.

31

32 **Acknowledgements**

33 We acknowledge support from an ARC Centre of Excellence "Stem Cells Australia" (SR110001002, E.W.) and a
34 National Health and Medical Research Council (NHMRC) Project grant (APP1082271, TMW). TMW is supported by a
35 NHMRC Career Development Fellowship (APP1105420).

36

37 **Competing interests**

38 The authors declare no competing financial interests.

39 Abstract

40 The complement system, typically associated with innate immunity, is emerging as a key controller
41 of non-immune systems including in development, with recent studies linking complement
42 mutations with neurodevelopmental disease. A key effector of the complement response is the
43 activation fragment C5a which, through its receptor C5aR1, is a potent driver of inflammation.
44 Surprisingly, C5aR1 is also expressed during early mammalian embryogenesis, however no clearly
45 defined function is ascribed to C5aR1 in development. Here we demonstrate polarized expression of
46 C5aR1 on the apical surface of mouse embryonic neural progenitor cells *in vivo*, and on human
47 embryonic stem cell derived neural progenitors. We further show that signaling of endogenous C5a
48 during mouse embryogenesis drives proliferation of neural progenitor cells within the ventricular
49 zone, and was required for normal brain histogenesis. C5aR1 signaling in neural progenitors was
50 dependent on atypical protein kinase C zeta (PKC ζ), a mediator of stem cell polarity, with C5aR1
51 inhibition reducing proliferation and symmetric division of apical neural progenitors in human and
52 mouse models. C5aR1 signaling was shown to promote the maintenance of cell polarity, with
53 exogenous C5a increasing the retention of polarized rosette architecture in human neural
54 progenitors following physical or chemical disruption. Transient inhibition of C5aR1 during
55 neurogenesis in developing mice led to behavioral abnormalities in both sexes and MRI-detected
56 brain microstructural alterations, in studied males, demonstrating a requirement of C5aR1 signaling
57 for appropriate brain development. This study thus identifies a functional role for C5a-C5aR1
58 signaling in mammalian neurogenesis, and provides mechanistic insight into recently identified
59 complement gene mutations and brain disorders.

60 **Significance Statement**

61 The complement system, traditionally known as a controller of innate immunity, now stands as a
62 multi-faceted signaling family with a broad range of physiological actions. These include roles in
63 the brain, where complement activation is associated with diseases including epilepsy and
64 schizophrenia. This study has explored complement regulation of neurogenesis, identifying a novel
65 relationship between the complement activation peptide C5a, and the neural progenitor proliferation
66 underpinning formation of the mammalian brain. C5a was identified as a regulator of cell polarity,
67 with inhibition of C5a receptors during embryogenesis leading to abnormal brain development and
68 behavioral deficits. This work demonstrates mechanisms through which dysregulation of
69 complement causes developmental disease, and highlights the potential risk of complement
70 inhibition for therapeutic purposes in pregnancy.

71 Introduction

72 The key complement activation fragment, anaphylatoxin C5a, and its primary receptor, C5aR1, play
73 pivotal roles in inflammation and immune defense. However, it is increasingly recognized that this
74 evolutionarily ancient system also possesses unexpected roles in development, such as in
75 morphogenesis, neurogenesis, migration, and neuronal synapse pruning (Hawksworth et al., 2016;
76 Gorelik et al., 2017). Defects in complement signaling have been associated with
77 neurodevelopmental abnormalities such as autism, schizophrenia, and 3MC syndrome (Corbett et
78 al., 2006; Rooryck et al., 2011; Sekar et al., 2016).

79 Despite these emerging developmental roles of complement, the functional role of C5aR1 in
80 embryonic development remains poorly defined. During organogenesis of *Xenopus* embryos, C5 is
81 expressed in the neural plate of the developing nervous system, (McLin et al., 2008) and in mice
82 and humans, C5 and C5aR1 are expressed in the developing neural tube (Denny et al., 2013).
83 Postnatally, C5a-C5aR1 expression continues in neural stem cells *in vitro*, is expressed in migrating
84 neuroblasts in response to ischemia (Rahpeymai et al., 2006), and promotes the proliferation of
85 progenitor cells within the external granular layer of the post-natal rat cerebellum (Bénard et al.,
86 2008). We also previously demonstrated that C5 and C5aR1 are expressed in human embryonic
87 stem cells, and can regulate pluripotency (Hawksworth et al., 2014). This early embryonic
88 expression pattern of C5aR1 in the absence of other factors of the canonical pathogen-initiated
89 complement cascade (Jeanes et al., 2015), suggests that C5aR1 signaling has adopted additional
90 roles in mammalian development beyond innate immunity. However, despite this clear expression
91 of C5a receptors during brain development, a neurodevelopmental role for C5a remains poorly
92 defined.

93 To investigate the role of C5aR1 in neural progenitor cell physiology we utilized both mouse
94 models and human embryonic stem (hES) cells differentiated to a stage resembling the ventricular
95 zone of the developing brain. In these hES-derived cultures, neural rosettes are formed that display

96 apical polarization and interkinetic nuclear migration of periluminal cells, similar to that seen
97 during neurulation and in the cortical ventricular zone (Shi et al., 2012; Ziv et al., 2015). The
98 signaling mechanisms in the control of rosette polarity are highly conserved and the localization of
99 the Par3/Par6/PKC ζ complex to the apical membrane is essential for self-renewal of neural
100 progenitors through the orchestration of the balance between symmetric and asymmetric division
101 (Fietz and Huttner, 2010). Here, we show that C5aR1 is a regulator of the apicobasal polarity of
102 neural stem cells and that the acute pharmacological blockade of C5aR1 signaling during
103 neurogenesis results in reduced ventricular zone proliferation and cerebral disorganization, leading
104 ultimately to behavioral alterations. Collectively our data reveal that C5aR1 functions as a regulator
105 of mammalian brain development under normal physiological conditions in both mice and humans.
106 This work complements recent studies documenting mutations in complement activation pathways
107 that contribute to an increased risk of neurodevelopmental disorders.

108 **Materials & Methods**

109 *Reagents*

110 Mouse recombinant C5a (mC5a) was obtained from Sigma Aldrich and reconstituted in 0.25% BSA
111 in PBS. Human isolated C5a (hC5a) was obtained from CompTech, USA. PMX53 was synthesized
112 as previously described (Pavlovski et al., 2012), stored lyophilized and reconstituted in purified
113 water before use.

114 *Tissue Collection and Processing*

115 All animal experiments in this study were performed with prior approval from the animal ethics
116 committee of the University of Queensland. Animal housing and time-mating of mice was
117 provided, with thanks, from University of Queensland Biological Resources. Tissues were collected
118 after sacrifice by cervical dislocation. Tissues preserved for RNA/protein analysis were snap frozen
119 in liquid nitrogen and stored at -80°C until extraction. Protein was extracted using modified RIPA
120 buffer prepared in-house. Tissues used for histological analysis were incubated at 4°C overnight in
121 freshly prepared 4% paraformaldehyde. Tissues were prepared for cryosection by sequential
122 passaging through serial sucrose solutions (10%, 20%, 30%), removed into OCT for freezing and
123 sectioned at 12µm, unless otherwise stated.

124 Embryonic cerebrospinal fluid (CSF) was obtained from E13.5 embryos using a pulled glass pipette
125 attached to a vacuum. Pooled CSF from three litters was used in analysis of mC5a concentration
126 through ELISA. CSF was treated with EDTA (5mM final concentration) to prevent coagulation and
127 extrinsic complement activation, and stored at -80°C until analysis.

128 *RT-PCR and qPCR*

129 RNA was extracted using RNeasy plus spin columns (QIAGEN, The Netherlands) and treated for
130 gDNA contamination using Turbo DNase (Life Technologies, USA). All RNA was additionally

131 checked for gDNA contamination by PCR analysis. Primer sequences and PCR conditions can be
132 found in Table 1. qPCR performed using SYBR green PCR mastermix (Ambion, USA) and
133 machine settings according to the manufacturer's instructions. The $\Delta\Delta Ct$ method to assess fold-
134 change of gene expression was employed and all data points within an individual sample were
135 referenced back to *r18s* expression levels.

136 *Western blot*

137 Protein samples (20 μ g) were subjected to electrophoresis at 100V on a 10% polyacrylamide gel
138 until good separation was achieved. Primary antibodies directed against C5aR1 (1:500, HBT clone
139 10/92, RRID:AB_10130226), phospho-Erk (1:1000, CST #9106, RRID:AB_331768), total-Erk
140 (1:1000, CST #9102, RRID:AB_330744) and beta-tubulin (1:2000, Sigma Aldrich clone TUB2.1,
141 AB_10679259) were diluted in 0.5x odyssey blocking buffer (LiCor, Germany) and incubated with
142 the membrane rocking overnight at 4°C. Incubation with specific Licor odyssey secondary
143 antibodies was carried out according to the manufacturer's instructions. Blots were imaged using the
144 Licor odyssey system and software. Optical densitometry values were derived from analysis of the
145 image in ImageJ (NIH, MD, USA, RRID:SCR_003070).

146 *Immunofluorescence*

147 Tissues or cells were blocked using 0.1% Triton X-100/4% goat serum in PBS for one hour. In the
148 case of live staining for NE-4C cultures, primary antibody was added to unfixed cells on ice for 30
149 minutes prior to fixation. Primary antibodies raised against mC5aR1 (HBT clone 10/92, 1:200,
150 RRID:AB_10130226), Pax6 (R&D #MAB1260, 1:500, RRID:AB_2159696), Phosphohistone H₃
151 (CST #9706, 1:1000, RRID:AB_331749), doublecortin (CST #4604, 1:500, RRID:AB_561007),
152 Sox2 (CST #3728, 1:500, RRID:AB_2194037), acetylated alpha-tubulin (Sigma Aldrich #T7451,
153 1:500, RRID:AB_609894), Zo-1 (Life Technologies, #402300, 1:500, RRID:AB_2533457),
154 hC5aR1 (BD, # 550733, 3 μ g/mL, RRID:AB_393854), C5 (HBT, clone bb5.1, 1:250,
155 RRID:AB_10992443), Tubb3 (Millipore, MAB1637, 1:1000, RRID:AB_2210524), NCAD (Sigma

156 Aldrich, C3865, 1:2000, RRID:AB_262097), Arl13b (NeuroMab, 73-287, 1:200,
157 RRID:AB_11000053), PKC ζ (Abcam, ab59412, 1:250, RRID:AB_946308) or isotype control
158 antibodies were incubated overnight at 4°C. Appropriate alexafluor secondary antibodies
159 (Invitrogen, USA, 1:1000) were incubated with the samples for 2 hours at room temperature before
160 counterstaining (1 μ g/mL DAPI, 5 min) and mounting. For C5aR/PKC ζ costaining, the issue of
161 using two rabbit antibodies was circumvented with the use of conjugated Fab fragments and
162 intermediate blocking with unconjugated Fab fragment (Jackson Lab, USA). All
163 immunofluorescence images were acquired via confocal microscopy (DMi8, Leica Microsystems,
164 Germany) and processed with ImageJ software. Further image analysis was performed with either
165 ImageJ or CellProfiler (Broad Institute, MA, USA, RRID:SCR_007358) software, as stated in the
166 relevant methods sections.

167 *mC5a ELISA*

168 Maternal and embryonic brain sample concentrations were determined by BCA assay
169 (ThermoScientific, USA). Aliquots of each sample were measured in technical triplicate for mC5a
170 concentration by enzyme-linked immunosorbent assay (R&D systems, USA, RRID:AB_2067297)
171 according to manufacturer's instructions. mC5a concentrations were normalized to protein
172 concentration (ng/mg, brain samples) or volume (ng/mL, CSF).

173 *Neurosphere culture*

174 Telencephalon from litters of E14.5 C57BL6/J mice, RRID:IMSR_JAX:000664, were isolated and
175 mechanically dissociated. Cells were maintained in DMEM/F12 media supplemented with 1x B27
176 supplement, L-glutamine 10ng/mL bFGF, 10ng/mL EGF and penicillin/streptomycin. Isolated
177 human rosettes were maintained in N2B27 throughout the neurosphere assay. To assess the effect of
178 C5aR1 modulation on neurosphere growth 10³ cells at passage 3 were seeded into each well of a 96
179 well plate in the presence or absence of 10nM mC5a. Wells were imaged after one week in culture

180 and the number and diameter of neurospheres assessed. Media was replaced every 48 hours. Before
181 treatment with 10nM mC5a cells were deprived of growth factors (bFGF/EGF) for 6 hours.

182 *NE-4C culture*

183 NE-4C cells were acquired from the American Type Culture Collection (#CRL-2925,
184 RRID:CVCL_B063) and expanded in MEM (Sigma Aldrich) supplemented with 10% FCS (Lonza,
185 Switzerland), L-glutamine and Non-essential amino acids (Life Technologies, USA). For transwell
186 culture, NE-4C cells were plated on poly-L-lysine coated 0.2 μ m transwell membranes in a 24-well
187 plate. Cells were maintained in media as described above and treatment (mC5a or vehicle) was
188 added to the upper compartment 12 hours before fixation for immunofluorescence.

189 *Human embryonic stem cell culture and neuronal differentiation*

190 H9 hES cells (RRID:CVCL_9773) were maintained on Matrigel (BD Biosciences, San Diego, CA)
191 coated dishes in mouse embryonic fibroblast conditioned KSR medium (Dulbecco's modified
192 Eagle's medium/F-12 supplemented with 20% Gibco KnockOut Serum Replacement, 0.1 mM
193 nonessential amino acids, 1 mM l-glutamine, 0.1 mM β -mercaptoethanol, and 10 ng/ml human
194 basic fibroblast growth factor [FGF2] - all sourced from ThermoFisher, USA) as previously
195 described (Briggs et al., 2013). Neuronal induction was performed using an adapted method of dual
196 SMAD inhibition (Chambers et al., 2009). Briefly, high density H9 cells were incubated for 10 days
197 in N2B27 medium (1:1 mixture of DMEM/F-12 supplemented with N2 and Neurobasal medium
198 supplemented with B27, 0.1 mM nonessential amino acids, 1 mM l-glutamine, 0.1 mM β -
199 mercaptoethanol, 50 U/ml penicillin, and 50 mg/mL streptomycin) supplemented with 1
200 μ M Dorsomorphin and 10 μ M SB431542. At day 10, cultures were bulk passaged using 1 mg/mL
201 dispase solution and seeded on Matrigel coated plates in N2B27 medium without Dorsomorphin
202 and SB431542. The cultures passaged again using a similar technique at day 15, maintaining bulk
203 and high density culture. Cells were supplemented with 2 ng/mL FGF2 from day 16 to day 22 to
204 promote emergence and proliferation of rosettes. Using this method, rosettes began to emerge

205 around day 16-18, reaching maturity 7 to 10 days later. In order to ensure purity of neuronal
206 cultures, rosettes were manually harvested around day 24.

207 *Human neural rosette experiments*

208 Rosette cultures were single cell dissociated with Accutase (ThermoFisher, USA) and seeded at
209 either high density (3.2×10^5 cells/cm 2) or low density (1.2×10^5 cells/cm 2) for subsequent
210 experiments. At high density, 100% of cells re-formed rosettes, allowing for experimentation on a
211 pure culture of uniformly sized rosettes. At low density, the ability of rosette re-formation was
212 limited (see results), allowing for interrogation of the ability of C5aR1 signaling to promote
213 reestablishment of rosettes over differentiation.

214 Low density single cells were grown for 7 days in the presence of 10 nM hC5a, 1 μ M PMX53 +
215 hC5a, or vehicle control, after which cells were fixed in 4% paraformaldehyde and stained for
216 NCAD using the above immunocytochemistry methods protocol. Acquired images were analyzed
217 using CellProfiler (RRID:SCR_007358) to quantify rosette number through the measurement and
218 quantification of NCAD positive rosette lumens (Kamentsky et al., 2011).

219 High density single cells were cultured for 5 days to allow re-establishment of rosettes after which
220 cells were tested in DAPT treatment and cell cycle progression experiments. For DAPT treatment,
221 cells were pre-treated with 10nM hC5a or vehicle control for 1 hour, after which 1 μ M DAPT was
222 added. Cells were incubated overnight, after which they were fixed, stained for NCAD, imaged, and
223 analyzed with CellProfiler to quantify rosette number or RNA collected for qRT-PCR. For cell
224 cycle testing, cells were serum starved overnight in DMEM/F12 + 0.25% BSA, after which 10nM
225 hC5a or vehicle control was added to the cells. The cells were then incubated overnight after which
226 they were fixed and stained with anti-pHH3 antibody and DAPI using the above
227 immunocytochemistry methods protocol. The ratio of pHH3 positive nuclei was calculated using
228 analysis with CellProfiler.

229 *In utero injections*

230 Time-mated dams at E13.5 were anaesthetized under 1% isofluorane for surgery. 1uL of 100nM
231 mC5a, 10 μ M PMX53 or respective vehicle control was injected into the ventricular system of the
232 embryos. Abdominal incisions were closed with sutures and dams were administered 0.1mg/kg
233 buprenorphine for analgesia post-surgery. Dams were sacrificed and tissues collected at 24-hours
234 post-surgery for tissue analysis.

235 For analysis of proliferation the embryonic telencephalon was sectioned coronally and sections at
236 the level of the preoptic area were used for histological analysis. M-phase cells, as determined by
237 phosphohistone H₃ staining, were counted using ImageJ at the apical surface of the telencephalic
238 ventricular zone. Phosphohistone H₃ positive cells per 100 μ m was calculated for each individual
239 embryo and differences between treatment groups analyzed by students T-test.

240 *Treatment of animals for behavioral experiments and MRI*

241 Time-mated dams were acquired from UQBR and housed under standard conditions under the care
242 of animal house staff. Mice were administered 1mg/kg PMX53 or sterile water vehicle control (n=6
243 per group) in a 100 μ L volume via intraperitoneal injection over three days (E12.5 - E14.5). Dams
244 were allowed to litter down in individual cages. Gestational age at birth was defined as the number
245 of days after discovery of the vaginal plug (E0.5). Litter number, weight, crown-rump length and
246 snout-occiput length were taken at birth. In addition, pup weight was tracked over the first five
247 weeks of life to determine if any differences existed in growth parameters.

248 At eight weeks of age male and female mice from the litters were randomly selected for
249 participation in behavioral experiments (n = 8 per group). After behavioral experiments mice were
250 anaesthetized with zylazine/xoletil cocktail and perfused with PBS followed by 4% PFA via an
251 intracardiac cannula. Whole heads were incubated in 4% PFA for a further 3 days before washes
252 with PBS and careful removal of the brain. Brains were stored in fresh PBS until MRI analysis.

253 *Grip strength*

254 Mice were assessed for motor weakness using the grip strength test. Briefly, mice gripped a bar
255 attached to a force transducer. The experimenter gently pulled backwards on the base of the tail
256 until the mouse dislodged from the bar. The maximum force recorded over three trials was
257 designated as the grip strength. Both forelimb and hindlimb grip strength was assessed.

258 *Balance Beam*

259 Mice were assessed for higher motor coordination using the balance beam test. The apparatus
260 consisted of a 70cm (length) x 3mm (width) beam suspended 1m above a surface. The beam was
261 held in a room with bright overhead lights kept at a constant output of 150 lumens, a covered
262 platform was set at the end of the beam. Mice were trained, through four training attempts, to move
263 towards the covered platform through the use of a training beam of 80mm width. After training,
264 mice were exposed to the test apparatus. Time taken to cross beam and foot fall errors were
265 recorded. A footfall error was deemed to have occurred if the paw of the animal moved from a
266 position on the beam and crossed a threshold 10mm beneath the beam.

267 *Open Field Test*

268 The open field test utilized 50 x 50cm infrared photobeam tracking arenas (Med associates, USA) to
269 measure activity in a novel environment. Mice were placed in the center of the arena and, after a
270 30s initiation period, movement in the x, y and z planes was tracked for the following 30 minutes.
271 Arenas were cleaned with 70% ethanol and allowed to dry between experiments. Thigmotaxis over
272 the initially 5 minutes was used as a measure of anxiety in the new environment and was assessed
273 as beam breaks within the center (25 x 25cm) square of the arena.

274 *Y-maze*

275 The Y-maze consisted of a Y shaped maze of opaque white plastic with three identical arms set at
276 120° angles. The arms were consisted of a home arm, of plain design and two exploratory arms
277 where the walls were decorated with different repetitive geometric patterns. For the exploratory

278 task, one exploratory arm was blocked from the maze by use of a plastic divider. A subject was
279 placed in the home arm and allowed to explore the home arm and remaining exploratory arm for 5
280 minutes. The subject was then re-introduced to the maze after a 30-minute period with the arm
281 divider removed, allowing for entry into the second, novel, exploratory arm. The movement of the
282 mouse around the maze was tracked with EthoVision video tracking software (Noldus, The
283 Netherlands). Frequency of entry into the novel arm was used as a measure of short term memory.

284

285 *MRI analysis of brain regions*

286 Brains stored for MRI analysis were washed extensively in PBS, followed by 48h incubation in
287 gadolinium contrast agent (0.2% Magnevist, Bayer Healthcare Pharmaceuticals, in PBS). Brains
288 were imaged on 16.4T small animal vertical wide bore NMR spectrometer (Bruker BioSpin) at the
289 Centre for Advanced Imaging, University of Queensland. Brains were immersed in fomblin oil
290 (Solvay Solexis, Italy) inside a glass test tube of 10mm diameter and fitted inside a quadrature
291 birdcage coil (M2M imaging Inc., USA). T₁ weighted images and multi-shell diffusion weighted
292 images (DWI) were obtained within a total scan time of 18 hours as previously described
293 (Sepherband et al., 2015). Briefly, DWI datasets were composed of three B₀ images and sixty
294 diffusion weighted images for each shell. Optimally ordered gradient directions with electrostatic
295 energy minimization were obtained using the Camino software package (Jones et al., 1999; Cook et
296 al., 2007).

297 Volumetric analysis of the obtained T₁ images was achieved using Advanced Normalisation Tools
298 (ANTs) software. Briefly, all T₁ images were warped to produce a common template image. Warp
299 fields containing Jacobian values for the individual images were subjected to a modified T-test
300 using the *randomize* function of FSL (Oxford center for functional MRI of the brain software
301 library, Oxford, UK) in order to determine significantly different Jacobian value voxels between the
302 vehicle and PMX53 treated groups. Inverse warp fields were applied to anatomical area mapping of

303 the common template to generate volumetric values for regions of sample brains. T₁ images and
304 generated anatomical masks were visualized and refined in ITKsnap software (University of
305 Pennsylvania, USA). Differences in brain regions volume were tested for using Student's T-test.

306 Images were registered using the FSL linear registration tool in order to compare anatomically
307 similar voxels between samples. Comparison of each of the diffusion parameters was achieved
308 using the *randomize* function of FSL to generate a probability map of differences between vehicle-
309 and PMX53-treated samples. Probability maps were thresholded to significance ($p \leq 0.05$) and
310 displayed on a generated template image.

311 *Statistical Analyses*

312 Graphing and statistics were performed using GraphPad Prism Software 6.0c (GraphPad Software,
313 USA) using Student's t test and one-way ANOVA with Dunnett post-test for the relevant statistical
314 analysis.

315 Results

316 *C5aR1 is expressed in murine neural progenitor cells and is localized to the apical ventricular*
317 *zone.*

318 We have previously reported the neuroepithelial expression of C5aR1 during mouse neurulation
319 (7.5-10.5 dpc) (Denny et al., 2013), but it is unknown if C5aR1 expression continues during the
320 period of neurogenesis. We therefore examined the temporal expression of C5aR1 in embryos 12.5-
321 18.5dpc. RT-PCR analysis of whole brain RNA extracts revealed *C5ar1* expression during this key
322 period of brain formation (Fig. 1A). Immunohistochemistry analysis indicated that C5aR1 protein
323 was distinctly localized to the apical surface of the ventricular zone (Fig. 1A). The ligand of C5aR1,
324 mC5a, was detected at very low levels in embryonic and adult brain tissue, however, it was found at
325 much higher levels in cerebrospinal fluid (CSF) sampled from E14.5 embryonic ventricles, but not
326 adult mouse CSF (Fig. 1D). Human concordance with these results has recently been reported, with
327 hC5a detected in the CSF of newborn infants (Pataky et al., 2016). Importantly, these embryonic
328 mC5a CSF concentrations equated to approximately 1.4nM, a functionally active concentration for
329 this potent signaling peptide (Hawksworth et al., 2014).

330 We next demonstrated that C5aR1 expression is maintained *ex vivo* in neurospheres derived from
331 the telencephalon of E14.5 mice, and the immortalized neural progenitor cell line NE-4C, as
332 determined by RT-PCR analysis (Fig. 1A) and immunocytochemistry (Fig. 1B&C). Interestingly,
333 differentiation of the NE-4C line with retinoic acid, confirmed by downregulation of *Sox2*, caused a
334 statistically significant reduction in C5aR1 mRNA between stage II and IV (Fig. 1F), a period that
335 corresponds to the beginning of neurogenesis and migration in the cultures (Schlett and Madarász,
336 1997). No reduction of C5aR1 protein was detected until stage VI, a period that marks the onset of
337 gliogenesis (Fig. 1E). The discordance in timing between mRNA and protein signal loss reflects
338 previous measurements of protein half-life in culture (Schwahnhäuser et al., 2011). Overall, this

339 indicates that C5aR1 retains a polarized localization in neural progenitor cells *ex vivo*, and
340 expression of the receptor reduces as cells differentiate.

341 *C5aR1 is apically localized in human embryonic stem cell-derived neural progenitors.*

342 To explore the role of C5aR1 in a human setting, we first assessed whether the mouse apical neural
343 localization of C5aR1 was conserved in human tissue. We have previously reported C5aR1
344 expression in a similar localization to mouse, with staining for C5aR1 restricted to the cortical
345 ventricular zone of Carnegie stage 13 human neural tissue (Denny et al., 2013). To further assess
346 C5aR1 localization and function in human development, we utilized hES-derived neuronal
347 progenitors as an *in vitro* model system. To this end, hES cells were differentiated into cortical
348 neural rosettes, a stage with characteristics analogous to the cortical ventricular zone (Shi et al.,
349 2012; Ziv et al., 2015). The cells in these human neural rosettes expressed the neural markers
350 TUBB3 and NCAD, with strong expression of the tight junction marker ZO-1 on the apical luminal
351 surface of each rosette, indicative of the distinct apicobasal polarity that defines the rosette
352 architecture (Fig. 2A). C5aR1 expression was robustly detected at the apical surface of rosettes,
353 where it co-localized strongly with the apical membrane marker atypical protein kinase C zeta
354 (PKC ζ), but not with markers of cell-cell junctions (NCAD) or cilia (Arl13b), suggesting that the
355 protein is confined to the apical plasma membrane (Fig. 2A). In neural progenitor cells, the apical
356 membrane attachment acts as an anchor for determinants of polarity such as the Par3/Par6/PKC ζ
357 complex, which together with apical NCAD-based adherens junctions maintains tissue architecture
358 and apicobasal polarity (Götz and Huttner, 2005). Interestingly, we observed a close correlation
359 between NCAD and C5aR1 expression levels during the neural differentiation of hES cells.
360 Upregulation of NCAD after neural induction peaked at the rosette stage and decreased upon further
361 maturation of the cultures. Both C5aR1 and C5 closely followed this pattern of expression (Fig.
362 2B). C5 protein expression appeared diffuse and punctate throughout the rosettes (Fig. 2A), and the
363 processed form of C5, hC5a, was detectable in the lysate of rosette cells at a similar time-point (Fig.

364 2C). High lysate levels of C5a may reflect intracellular stores of C5a, as has been observed and
365 discussed previously for the complement anaphylatoxins (Pavlovski et al., 2012; Hawksworth et al.,
366 2014; Elvington et al., 2017). These results indicate that human subcellular and temporal C5aR1
367 expression during development closely mirrors that observed in developing mouse brain.

368

369 *C5aR1 signals via PKCζ and Erk in mouse and human neural progenitors to promote polarization*
370 *and proliferation.*

371 Intrigued by the unique apical localization of C5aR1 *in vivo* and *in vitro*, and the well described
372 importance of the apical membrane and *PKCζ* in controlling progenitor pool proliferation, we next
373 assessed the functional role of C5aR1 in these processes. In mouse neurosphere cultures, mC5a
374 addition caused an increase in p42/44 (ERK) phosphorylation (Fig. 3A), which could be effectively
375 inhibited through pretreatment with a specific *PKCζ* pseudosubstrate inhibitor (Fig. 3B). Similarly,
376 in human rosette cultures, treatment with human C5a caused an increase in p42/44 phosphorylation
377 that was attenuated through pretreatment with either a selective C5aR1 antagonist (C5aR1-A,
378 PMX53), or with *PKCζ* inhibition (Fig. 3C), indicating that C5aR1 signaling is conserved between
379 human and mouse. Given the association between ERK signaling and mitogenic activity, we
380 investigated the ability of C5aR1 signaling to modulate neural progenitor proliferation. Daily
381 addition of species-specific C5a to neurosphere cultures resulted in an increase in both number and
382 diameter of mouse and human neurospheres over a 7-day period (Fig 3D/E & F/G respectively).
383 Additionally, in human neural rosette cultures, addition of C5a led to a 59% increase in
384 phosphorylated histone H3 (pHH3) positive nuclei, indicative of increased mitotic activity within
385 rosettes (Fig. 3H).

386

387 The observation that C5aR1 signaling is mediated by *PKCζ*, a component of the Par3/Par6/*PKCζ*
388 cell polarity complex, combined with its localization at the apical membrane of neural rosettes,

389 strongly supports a role for C5aR1 in controlling neural progenitor cell (NPC) polarity. We
390 therefore examined a role of C5aR1 in NPC polarity signaling pathways. Previous studies have
391 shown that a loss of paracrine Notch signaling results in downregulation of NCAD and the loss of
392 apicobasal polarity (Main et al., 2013). Treatment of human neural rosettes with the Notch signaling
393 inhibitor DAPT significantly decreased the expression of NCAD, leading to a disruption of cell-cell
394 contacts and induced a loss of rosette architecture (Fig. 3I). Interestingly both C5aR1 and C5
395 expression also decreased with DAPT treatment, which may indicate polarity-dependent expression
396 of these complement factors (Fig. 3I). Single cell dissociation of rosettes also interferes with
397 paracrine signaling and cell-cell contact, resulting in loss of cell polarity and impaired rosette
398 formation. Exogenous addition of hC5a maintained rosette architecture in the presence of DAPT
399 (Fig. 3J), and promoted re-establishment of rosette architecture after dissociation, an effect that was
400 blocked following C5aR1 antagonism (Fig. 3K). We conclude that C5aR1 is not only dependent on,
401 but also actively promotes, cell polarity.

402

403 This promotion of polarity was also observed in mouse-derived NE-4C cells cultured on transwell
404 plates. Addition of exogenous mC5a led to restriction of the apical surface area by ~50%, as
405 measured by ZO-1 staining, and microtubule organizing center (MTOC) localization in these cells
406 was significantly closer to the apical center, indicative of the induction of cell polarization (Fig.
407 3L&M). Collectively, these data confirmed the polarity-dependent expression of C5aR1, an
408 involvement of C5aR1 signaling in the maintenance of neural progenitor polarity, and subsequently,
409 proliferation.

410

411 *C5aR1 signaling increases the proliferation of neural progenitor cells of the embryonic ventricular
412 zone in vivo*

413 Having defined a role for C5aR1 in NPC proliferation and establishment of cell polarity *in vitro*, we
414 next wished to assess its role in mouse brain development by *in utero* delivery of mC5a or C5aR1-
18

415 A (PMX53) into the embryonic ventricle of embryonic day (E)13.5 mouse embryos (Fig. 4A). We
416 observed that twenty-four hours after a single injection with mC5a there was a 2-fold increase in the
417 number of apical progenitors in M-phase of the cell cycle, as indicated by pHH3 staining (Fig. 4B).
418 In contrast, blockade of C5aR1 signaling resulted in a decrease in the number of M-phase apical
419 progenitors after 24 hours (Fig. 4B). Analysis of the cleavage plane of actively dividing cells in
420 these samples demonstrated a significant shift from symmetric to asymmetric division following
421 C5aR1-A injection (Fig. 4C). We conclude that C5aR1 signaling promotes NPC proliferation *in*
422 *vivo* and affects the balance between symmetric and asymmetric division, in concordance with *in*
423 *vitro* observations. Combined with the robust expression of mC5a in embryonic CSF (Fig. 1D), this
424 supports an endogenous physiological role for mC5a-C5aR1 signaling during embryonic
425 neurogenesis.

426

427 *Blockade of C5aR1 from E12.5-14.5 results in behavioral abnormalities in the adult mouse*

428 Given that acute disruption of C5a-C5aR1 signaling affects proliferation of apical progenitors and
429 the balance between symmetric and asymmetric cell division, we next determined whether acute
430 pharmacological blockade of C5aR1 during neurogenesis translates into behavioral abnormalities
431 later in life. Time-mated dams were intraperitoneally injected daily with 1mg/kg C5aR1-A during
432 the critical neurodevelopmental window (E12.5-14.5), and resultant litters were subjected to
433 behavioral testing between 6-8 weeks of age (Fig. 5A). We first confirmed that intraperitoneal
434 delivery of C5aR1-A over the three-day embryonic window resulted in impaired neurogenesis.
435 Compared to vehicle controls C5aR1-A-treated embryos displayed a reduction in the size of the
436 ventricular zone, as measured by Sox2 staining, and an increase in the thickness of the maturing
437 cortex, as demonstrated by the post-mitotic maturing neuron marker doublecortin (DCX) at E16.5.
438 This collectively resulted in a significant decrease of the Sox2/DCX ratio (Fig. 5B). We next
439 assessed whether C5aR1-A treatment resulted in any gross developmental or pregnancy

440 complications. C5aR1-A treated pups showed no change in postnatal growth (Fig. 5C), litter size
441 (Fig. 5D) and snout-occiput length (Fig. 5F), however a minor, but significant, reduction in crown-
442 rump length was observed (Fig. 5E).

443

444 Adult mice were next subjected to a series of behavioral tests to assess neuromotor and cognitive
445 function. *In utero* C5aR1-A treated mice demonstrated significant behavioral abnormalities in
446 adulthood. In motor control tasks, there was no difference in grip-strength (Fig. 5G), however
447 balance beam testing of centrally-controlled motor coordination tasks showed an increase in both
448 footfall errors and time taken to cross the beam for C5aR1-A treated mice (Fig. 5H, I). In an open
449 field test, C5aR1-A treated animals of both genders demonstrated a decrease in distance travelled in
450 the center areas of the cage (Fig. 5J), suggesting heightened anxiety in a novel environment. The Y-
451 maze was used to assess short-term memory, and frequency of entry into the novel arm was reduced
452 in C5aR1-A treated animals (Fig. 5K). Finally, the forced swim test was used to assess depressive-
453 like symptoms, where C5aR1-A treated animals spent significantly reduced time being immobile
454 compared to non-treated animals (Fig. 5L). These results clearly demonstrated that acute *in utero*
455 blockade of C5aR1 signaling over a relatively short time frame led to a range of behavioral
456 discrepancies that involved several anatomically distinct systems such as memory, coordination and
457 anxiety.

458

459 *In utero blockade of C5aR1 between E12.5-14.5 results in microstructural differences on MRI*
460 *analysis*

461 Given the broad behavioral deficits induced by transient *in utero* C5aR1 antagonism between
462 E12.5-14.5 of gestation, we next utilized *ex vivo* 16.4T magnetic resonance imaging (MRI) to
463 identify structural alterations in the brain that could underlie the observed phenotypes. Firstly, a
464 Jacobian map was utilized to measure the relative change of each brain structure required to fit to a

465 template image, therefore identifying any volumetric change in distinct regions between sample
466 groups (Leporé et al., 2007). C5aR1-A treated animals showed significantly increased clusters of
467 Jacobian values throughout the cortex and striatum (Fig. 6) indicating that spatial expansion was
468 required to fit individual images to the template in these areas (Lepore et al., 2008). However,
469 volumetric analysis of segmented brain regions (Ma et al., 2005) failed to show significant
470 differences between groups (Table 2). These areas of volume difference correlated with
471 microstructural difference as shown by fractional anisotropy (FA). FA values were higher in the
472 frontal cortex, striatum, and hypothalamus of C5aR1-A treated animals (Fig. 6) alluding to
473 increased myelination, increased axonal density or a reduction in fiber dispersion in these areas
474 (Sepehrband et al., 2015), which may account for the behavioral differences seen between these two
475 experimental groups (Soares et al., 2013). Overall, these results demonstrate multiple
476 microstructural differences induced by C5aR1 inhibition in embryos, which are concordant with the
477 behavioral deficits seen in these mice.

478 Discussion

479 Proteins of the complement system are present during embryogenesis, playing novel roles in
480 development (McLin et al., 2008; Denny et al., 2013; Jeanes et al., 2015). Our laboratory has
481 previously demonstrated their presence and function on human embryonic stem cells and mouse
482 neuroepithelial cells (Denny et al., 2013; Hawksworth et al., 2014). Additionally, we have
483 previously shown C5aR1 expression on the apical neuroepithelium at a similar developmental stage
484 to this study, in non-pathological human embryos (Denny et al., 2013), raising the question of roles
485 for complement in normal embryonic development. Here we show that in both human and mouse
486 models, the key complement effector system, C5a-C5aR1 signaling, functions to control progenitor
487 cell polarity, proliferation and the symmetry of the cell division. Ultimately, this loss of C5aR1
488 signaling manifests as altered cerebral organization and behavioral deficits.

489 In neural progenitor cells of the ventricular zone, the loss of apical attachment where C5aR1 resides
490 is associated with decreased expression of factors responsible for the maintenance of stemness.
491 Asymmetric inheritance of this attachment during mitosis is a catalyst for differentiation toward a
492 post-mitotic state, with loss of attachment initiating exit from the ventricular zone pool, and
493 subsequent maturation into neuronal subtypes (Götz and Huttner, 2005; Miyamoto et al., 2015).
494 Conversely, symmetric division of the apical membrane maintains both daughter cells within the
495 ventricular zone progenitor pool, secondary to continued signaling from the apical membrane. The
496 apically-localized PKC ζ is an essential second messenger in the promotion of symmetric division
497 and the maintenance of neuroepithelial architecture (Ghosh et al., 2008). However, less is known
498 about the receptors that trigger PKC ζ activation. Here we have identified C5aR1 as a novel prime
499 candidate, with polarized apical expression, for controlling endogenous PKC ζ signaling during
500 mammalian corticogenesis.

501 In addition, we have shown a plausible biological source for C5aR1 stimulation within the CSF of
502 the developing embryo, which were at higher concentrations than both embryonic brain tissue and
22

503 adult CSF. This may suggest that C5a is actively secreted into the CSF to stimulate proliferation of
504 progenitor cells, given that concentrations are higher during development than in adulthood. The
505 source of this C5a will require further delineation, however we demonstrated C5 expression within
506 neural rosette cultures (Fig 2A). As the CSF was assayed before the advent of ependymal cell
507 differentiation, this strongly suggests an autocrine production of C5a by neural progenitor cells.

508 These findings are particularly of interest in light of previous reports demonstrating that, in adult
509 mice, C5aR1 does not contribute to basal neurogenesis (Bogestål et al., 2007). This appears to
510 contrast with our study, which identifies a role for C5aR1 in neurogenesis, albeit at an earlier stage
511 of life than investigated by Bogestål and colleagues (2007). However, the receptor has also been
512 demonstrated on migrating neuroblasts in models of cerebral ischemia (Rahpeymai et al., 2006),
513 leading to some question of its role on these cells, given an apparent non-contributory role to
514 neurogenesis. Whilst not directly tested, it could be argued that C5aR1 is responsive on neuroblasts
515 to the higher C5a concentrations in the ischemic brain, but has a dormant role in the non-
516 pathological, and therefore low-C5a, setting.

517 The present discovery adds to previous studies which have identified neurodevelopmental deficits
518 associated with aberrant complement activity, including in disorders such as autism, schizophrenia,
519 and epilepsy (Haworth et al., 2016). For example, the fetal neurocognitive injury associated
520 with maternal malaria infection has been shown to be mediated by C5aR1 (McDonald et al., 2015).
521 Furthermore, allele variations leading to increased complement factor 4A (C4A) expression have
522 been correlated to increased schizophrenia risk (Sekar et al., 2016). It is interesting to speculate,
523 given our findings, on whether the behavioral deficits demonstrated in both diseases are the result of
524 a direct effect of C5aR1 signaling on neural progenitors, altering corticogenesis, rather than the
525 alternate hypothesis of a generalized inflammation and altered synaptic pruning. Within this
526 hypothesis, classical complement cascade activation would inescapably lead to the formation of C5
527 convertases, and activation of C5. Given our identification of a mechanistic role for C5aR1 in

528 ventricular zone progenitors and cerebral organization, it could equally be hypothesized that the
529 increased C4A and classical complement cascade activation increases cerebral C5aR1 signaling,
530 with consequent alterations in progenitor migration driving the complex cortical pathology
531 associated with schizophrenia risk. Additionally, it is interesting that the short window of C5aR1
532 blockade used in our studies was also not compensated for later in development, as demonstrated by
533 the behavioral and brain microstructural differences in adult mice. In contrast, there is a
534 demonstrated functional compensation of impaired synaptic pruning resulting from other models of
535 complement deficiency (Perez-Alcazar et al., 2014). This theory is supported by the finding of
536 impaired short term memory in C5aR1 knockout animals (Gong et al., 2013), indicated that
537 disruption of the receptor signaling, but not the cascade, is enough to alter neuronal circuitry.

538 Given the potential disparity between animal and human cognitive development, one focus of this
539 study was to validate observations made in the mouse model in a human environment. We have
540 previously shown expression of C5aR1 in human embryos, at Carnegie stage 13, where it is also
541 localized to the apical neuroepithelium (Denny et al., 2013). The combination of this *in vivo*
542 localization with the results presented in this study, demonstrating human neural progenitors
543 signaling through C5aR1 in a similar manner to the mouse, strongly suggests conservation of
544 C5aR1 function between mouse and human. C5aR1 is already a strong candidate target for direct
545 therapeutics against inflammatory diseases of pregnancy. Maternal complement dysregulation is a
546 factor in the pathogenesis of preeclampsia and infection-related preterm birth (Lokki et al., 2014;
547 Denny et al., 2015). Interestingly, the humanized IgG2/4 monoclonal antibody directed against C5,
548 eculizimab, has already been in use in pregnant women affected by paroxysmal nocturnal
549 haemoglobinuria (PNH). Given the rarity of the disease there have only been a few reports on the
550 safety of this drug in pregnancy, with no obvious complications at birth nor in early childhood
551 development (Kelly et al., 2015). The effect of eculizimab is fortuitously confined to the maternal
552 circulation by the poor transfer of IgG2 through the placenta, and comparison of maternal and cord
553 blood from these pregnancies has shown no effect on the complement system of the fetus

554 (Hallstensen et al., 2015). However, with the clinical development of small molecule C5aR1
555 inhibitors, such as CCX-168 (Woodruff et al., 2011), it would be prudent to be cautious in the
556 clinical use of C5aR1 directed therapeutics during pregnancy without prior consideration to fetal
557 transfer and potential developmental implications of C5aR1 inhibition as highlighted in this study.

558 This study also adds to emerging work demonstrating a wide developmental role for complement
559 components in mammalian development. These include roles for complement factors in
560 developmental processes such as radial intercalation, migration and synaptic pruning (Stevens et al.,
561 2007; Carmona-Fontaine et al., 2011; Szabó et al., 2016; Gorelik et al., 2017). In this context, it is
562 interesting to speculate what niche these proteins first filled. The origins of the evolutionarily
563 ancient system of complement proteins may be as a controller of tissue organization and
564 development, with utilization of complement in the context of innate immunity following later in
565 evolution (Hawksworth et al., 2016).

566 In conclusion, here we show a novel role for C5aR1 as a modulator of apicobasal polarity in neural
567 progenitor cells that is highly conserved between mice and humans. Inhibition of C5aR1 signaling
568 during neurogenesis has deleterious consequences for cerebral organization, resulting in behavioral
569 abnormalities in adult mice. Our data suggest that the development and use of C5aR1 antagonists as
570 potential treatments for pregnancy-related inflammatory disease should be approached with extreme
571 caution.

572 **References**

- 573 Bénard M, Raoult E, Vaudry D, Leprince J, Falluel-Morel A, Gonzalez BJ, Galas L, Vaudry H,
574 Fontaine M (2008) Role of complement anaphylatoxin receptors (C3aR, C5aR) in the
575 development of the rat cerebellum. *Mol Immunol* 45:3767–3774.
- 576 Bogestål YR, Barnum SR, Smith PLP, Mattisson V, Pekny M, Pekna M (2007) Signaling through
577 C5aR is not involved in basal neurogenesis. *J Neurosci Res* 85:2892–2897.
- 578 Briggs JA, Sun J, Shepherd J, Ovchinnikov DA, Chung TL, Nayler SP, Kao LP, Morrow CA,
579 Thakar NY, Soo SY, Peura T, Grimmond S, Wolvetang EJ (2013) Integration-Free Induced
580 Pluripotent Stem Cells Model Genetic and Neural Developmental Features of Down Syndrome
581 Etiology. *Stem Cells* 31:467–478.
- 582 Carmona-Fontaine C, Theveneau E, Tzekou A, Tada M, Woods M, Page KM, Parsons M, Lambris
583 JD, Mayor R (2011) Complement Fragment C3a Controls Mutual Cell Attraction during
584 Collective Cell Migration. *Dev Cell*.
- 585 Chambers SM, Fasano CA, Papapetrou EP, Tomishima M, Sadelain M, Studer L (2009) Highly
586 efficient neural conversion of human ES and iPS cells by dual inhibition of SMAD signaling.
587 *Nat Biotechnol* 27:275–280.
- 588 Cook PA, Symms M, Boulby PA (2007) Optimal acquisition orders of diffusion-weighted MRI
589 measurements. *J Mag Reson Im* 25:1051-1058.
- 590 Corbett BA, Kantor AB, Schulman H, Walker WL, Lit L, Ashwood P, Rocke DM, Sharp FR (2006)
591 A proteomic study of serum from children with autism showing differential expression of
592 apolipoproteins and complement proteins. *Mol Psychiatry* 28:355.
- 593 Denny KJ, Coulthard LG, Jeanes A, Lisgo S, Simmons DG, Callaway LK, Wlodarczyk B, Finnell
594 RH, Woodruff TM, Taylor SM (2013) C5a receptor signaling prevents folate deficiency-
595 induced neural tube defects in mice. *J Immunol* 190:3493–3499.
- 596 Denny KJ, Coulthard LG, Mantovani S, Simmons D, Taylor SM, Woodruff TM (2015) The Role of
597 C5a Receptor Signaling in Endotoxin-Induced Miscarriage and Preterm Birth. *Am J Repro
598 Immunol* 74:148–155.
- 599 Elvington M, Liszewski MK, Bertram P, Kulkarni HS, Atkinson JP (2017) A C3(H2O) recycling
600 pathway is a component of the intracellular complement system. *J Clin Invest* 127(3):970-981.
- 601 Fietz SA, Huttner WB (2010) Cortical progenitor expansion, self-renewal and neurogenesis-a
602 polarized perspective. *Curr Opin Neurobiol* 21:23-35.
- 603 Ghosh S, Marquardt T, Thaler JP, Carter N, Andrews SE, Pfaff SL, Hunter T (2008) Instructive role
604 of aPKC ζ ta subcellular localization in the assembly of adherens junctions in neural
605 progenitors. *Proc Natl Acad Sci USA* 105:335–340.
- 606 Gong B, Pan Y, Zhao W, Knable L, Vempati P, Begum S, Ho L, Wang J, Yemul S, Barnum S,
607 Bilski A, Gong BY, Pasinetti GM (2013) IVIG immunotherapy protects against synaptic
608 dysfunction in Alzheimer's disease through complement anaphylatoxin C5a-mediated AMPA-
609 CREB-C/EBP signaling pathway. *Mol Immunol* 56:619–629.
- 610 Gorelik A, Sapir T, Haffner-Krausz R, Olender T, Woodruff TM, Reiner O (2017) Developmental

- 611 activities of the complement pathway in migrating neurons. *Nature Communications*. DOI:
612 10.1038/ncomms15096.
- 613 Götz M, Huttner WB (2005) The cell biology of neurogenesis. *Nat Rev Mol Cell Biol* 6:777–788.
- 614 Hallstensen RF, Bergseth G, Foss S, Jæger S, Gedde-Dahl T, Holt J, Christiansen D, Lau C, Brekke
615 O-L, Armstrong E, Stefanovic V, Andersen JT, Sandlie I, Mollnes TE (2015) Eculizumab
616 treatment during pregnancy does not affect the complement system activity of the newborn.
617 *Immunobiol* 220:452–459.
- 618 Hawksworth OA, Coulthard LG, Taylor SM, Wolvetang EJ, Woodruff TM (2014) Brief report:
619 complement C5a promotes human embryonic stem cell pluripotency in the absence of FGF2.
620 *Stem Cells* 32:3278–3284.
- 621 Hawksworth OA, Coulthard LG, Woodruff TM (2017) Complement in the fundamental processes
622 of the cell. *Mol Immunol* 84:17–25.
- 623 Jeanes A, Coulthard LG, Mantovani S, Markham K (2015) Co-ordinated expression of innate
624 immune molecules during mouse neurulation. *Mol Immunol* 68:253–260.
- 625 Jones DK, Horsfield MA, Simmons A (1999) Optimal strategies for measuring diffusion in
626 anisotropic systems by magnetic resonance imaging. *Magn Reson Med* 42:515–525.
- 627 Kamentsky L, Jones TR, Fraser A, Bray M-A, Logan DJ, Madden KL, Ljosa V, Rueden C, Eliceiri
628 KW, Carpenter AE (2011) Improved structure, function and compatibility for CellProfiler:
629 modular high-throughput image analysis software. *Bioinformatics* 27:1179–1180.
- 630 Kelly RJ, Höchsmann B, Szer J, Kulasekararaj A, de Guibert S, Röth A, Weitz IC, Armstrong E,
631 Risitano AM, Patriquin CJ, Terriou L, Muus P, Hill A, Turner MP, Schrezenmeier H, Peffault
632 de Latour R (2015) Eculizumab in Pregnant Patients with Paroxysmal Nocturnal
633 Hemoglobinuria *N Engl J Med* 373:1032–1039.
- 634 Leporé N, Brun C, Yi-Yu Chou, Ming-Chang Chiang, Dutton RA, Hayashi KM, Luders E, Lopez
635 OL, Aizenstein HJ, Toga AW, Becker JT, Thompson PM (2008) Generalized Tensor-Based
636 Morphometry of HIV/AIDS Using Multivariate Statistics on Deformation Tensors. *IEEE Trans
637 Med Imaging* 27:129–141.
- 638 Leporé N, Brun C, Pennec X, Chou Y-Y, Lopez OL, Aizenstein HJ, Becker JT, Toga AW,
639 Thompson PM (2007) Mean Template for Tensor-Based Morphometry Using Deformation
640 Tensors. In: *Medical Image Computing and Computer-Assisted Intervention MICCAI. Lecture
641 notes in computer science*, vol. 4792. Springer, Berlin, Heidelberg.
- 642 Lokki AI, Heikkinen-Eloranta J, Jarva H, Saisto T, Lokki M-L, Laivuori H, Meri S (2014)
643 Complement activation and regulation in preeclamptic placenta. *Front Immunol* 5:312.
- 644 Ma Y, Hof PR, Grant SC, Blackband SJ, Bennett R, Slates L, McGuigan MD, Benveniste H (2005)
645 A three-dimensional digital atlas database of the adult C57BL/6J mouse brain by magnetic
646 resonance microscopy. *Neurosci* 135:1203–1215.
- 647 Main H, Radenkovic J, Jin S-B, Lendahl U, Andersson ER (2013) Notch signaling maintains neural
648 rosette polarity. *PLoS ONE* 8:e62959.
- 649 McDonald CR, Cahill LS, Ho KT, Yang J, Kim H, Silver KL, Ward PA, Mount HT, Liles WC,
650 Sled JG, Kain KC (2015) Experimental Malaria in Pregnancy Induces Neurocognitive Injury in

- 651 652 Uninfected Offspring via a C5a-C5a Receptor Dependent Pathway Mota MM, ed. PLoS Pathog
11:e1005140–23.
- 653 654 McLin VA, Hu C-H, Shah R, Jamrich M (2008) Expression of complement components coincides
with early patterning and organogenesis in *Xenopus laevis*. *Int J Dev Biol* 52:1123–1133.
- 655 656 Miyamoto Y, Sakane F, Hashimoto K (2015) N-cadherin-based adherens junction regulates the
maintenance, proliferation, and differentiation of neural progenitor cells during development.
Cell Adh Migr 9:183–192.
- 657
- 658 659 Pataky R, Howie FA, Girardi G, Boardman JP (2016) Complement C5a is present in CSF of human
newborns and is elevated in association with preterm birth. *J Matern Fetal Neonatal Med*:1–4.
- 660 661 Pavlovski D, Thundyil J, Monk PN, Wetsel RA, Taylor SM, Woodruff TM (2012) Generation of
complement component C5a by ischemic neurons promotes neuronal apoptosis. *FASEB J*
26(9):3680–3690.
- 662
- 663 Perez-Alcazar M, Daborg J, Stokowska A, Wasling P, Björefeldt A, Kalm M, Zetterberg H,
Carlström KE, Blomgren K, Ekdahl CT, Hanse E, Pekna M (2014) Altered cognitive
performance and synaptic function in the hippocampus of mice lacking C3. *Exp Neurol*
253:154–164.
- 664
- 665
- 666
- 667 Rahpeymai Y, Hietala MA, Wilhelmsson U, Fotheringham A, Davies I, Nilsson A-K, Zwirner J,
Wetsel RA, Gerard C, Pekny M, Pekna M (2006) Complement: a novel factor in basal and
ischemia-induced neurogenesis. *EMBO J* 25:1364–1374.
- 668
- 669
- 670 Rooryck C et al. (2011) Mutations in lectin complement pathway genes COLEC11 and MASP1
cause 3MC syndrome. *Nat Genet* 43:197–203.
- 671
- 672 Schlett K, Madarász E (1997) Retinoic acid induced neural differentiation in a neuroectodermal cell
line immortalized by p53 deficiency. *J Neurosci Res* 47:405–415.
- 673
- 674 Schwahnhäuser B, Busse D, Li N, Dittmar G, Schuchhardt J, Wolf J, Chen W, Selbach M (2011)
Global quantification of mammalian gene expression control. *Nature* 473:337–342.
- 675
- 676 Sekar A, Bialas AR, de Rivera H, Davis A, Hammond TR, Kamitaki N, Tooley K, Presumey J,
Baum M, Van Doren V, Genovese G, Rose SA, Handsaker RE, Consortium SWGOTPG, Daly
MJ, Carroll MC, Stevens B, McCarroll SA (2016) Schizophrenia risk from complex variation
of complement component 4. *Nature* 530:177–183.
- 677
- 678
- 679
- 680 Sephrband F, Clark KA, Ullmann JFP, Kurniawan ND, Leanage G, Reutens DC, Yang Z (2015)
Brain tissue compartment density estimated using diffusion-weighted MRI yields tissue
parameters consistent with histology. *Hum Brain Mapp* 36:3687–3702.
- 681
- 682
- 683 Shi Y, Kirwan P, Smith J, Robinson HPC, Livesey FJ (2012) Human cerebral cortex development
from pluripotent stem cells to functional excitatory synapses. *Nat Neurosci* 15:477–86–S1.
- 684
- 685 Soares JM, Marques P, Alves V (2013) A hitchhiker's guide to diffusion tensor imaging. *Front*
Neurosci 12:7-31.
- 686
- 687 Stevens B, Allen NJ, Vazquez LE, Howell GR, Christopherson KS, Nouri N, Micheva KD,
Mehalow AK, Huberman AD, Stafford B, Sher A, Litke AM, Lambris JD, Smith SJ, John
SWM, Barres BA (2007) The classical complement cascade mediates CNS synapse
elimination. *Cell* 131:1164–1178.
- 688
- 689
- 690

- 691 Szabó A, Cobo I, Omara S, McLachlan S, Keller R, Mayor R (2016) The Molecular Basis of Radial
692 Intercalation during Tissue Spreading in Early Development. *Dev Cell* 37:213–225.
- 693 Woodruff TM, Nandakumar KS, Tedesco F (2011) Inhibiting the C5-C5a receptor axis. *Mol*
694 *Immunol* 48:1631–1642.
- 695 Ziv O, Zaritsky A, Yaffe Y, Mutukula N, Edri R, Elkabetz Y (2015) Quantitative Live Imaging of
696 Human Embryonic Stem Cell Derived Neural Rosettes Reveals Structure-Function Dynamics
697 Coupled to Cortical Development. *PLoS Comp Biol* 11:e1004453.

698

699 **Fig. Legends**

700 **Fig. 1; Localization of C5aR1 and ligands.** A) C5aR1 (red) is expressed in the developing
701 neocortex at the apical surface of the ventricular zone from at E14.5 (top row). Counterstain with
702 Pax6 (green), DAPI (blue). Scale bar = 50 μ m. Merged images of the ventricular zone at E12.5,
703 E16.5 and E18.5 are shown in the second row. RT-PCR demonstrates C5aR1 expression in
704 embryonic brain tissue, neurosphere and NE- 4C culture. B) C5aR1 expression (red) within
705 sectioned neurosphere. Secondary-only negative controlled labelled ‘Negative’. Scale bar = 50 μ m.
706 C) C5aR1 expression (red) on NE4C cells grown in monolayer. Secondary-only negative controlled
707 labelled ‘Negative’. Scale bar = 20 μ m. D) Embryonic CSF contains mC5a at significantly greater
708 concentrations than brain tissue or maternal CSF. E) C5aR1 is detected within NE-4C cultures by
709 western blot at the predicted molecular weight (50kDa), and decreases at stage VI of differentiation.
710 Stages indicate morphologically distinct progression of NE-4C differentiation (See Methods). F)
711 Expression of C5aR1 mRNA decreases with differentiation of NE-4C cells. Progenitor marker Sox2
712 is assayed as comparison.

713

714 **Fig. 2; Expression of C5aR1 in human embryonic stem cell-derived rosettes.** A)
715 Immunocytochemistry of human neural rosettes showing staining for neural marker TUBB3, tight
716 junction marker ZO-1, and complement factor 5 (C5). C5aR1 localizes to the apical membrane,
717 colocalizing with PKC ζ , but not markers of cilia (Arl13b) or tight junctions (NCAD). Negative
718 controls shown top right. Scale bar = 20 μ m. B) Transcript expression as human embryonic stem
719 (hES) cells (day 0) are differentiated through the cortical rosette stage (day 28) to a mature neuronal
720 lineage. *C5AR1* expression is highest at the rosette stage of neuronal differentiation. C) hC5a is
721 detected through ELISA within the lysate of rosette cultures, and is not derived from the exogenous
722 extracellular matrix (Matrigel).

723

724 **Fig. 3; C5aR1 signals through PKC ζ to maintain cell polarity *in vitro*.** A) Mouse neurosphere
725 cultures demonstrate C5a-concentration dependent p42/44 phosphorylation B) The response to
726 100nM C5a is prevented by PKC ζ inhibition. C) Human rosette cultures demonstrate time-
727 dependent p42/44 phosphorylation to 10nM hC5a. The response is prevented through pretreatment
728 with C5aR1-A or PKC ζ inhibition. D-G) Mouse and human neurosphere cultures dissociated and
729 grown over a 7-day period demonstrate an increase in number (D & F respectively) and diameter (E
730 & G respectively) in response to C5a. H-K) Treatment of human rosettes with 10nM C5a. H) C5a
731 increases M-phase positive cells in neural rosettes as determined by pHH₃ immunocytochemical
732 analysis. I) DAPT (grey bars) treatment induced loss of rosettes and decrease in mRNA of *NCAD*,
733 *C5ARI*, and *C5* compared to vehicle (black bars) treatment. Maintenance of rosette architecture
734 following single cell dissociation (K) or DAPT treatment (J) was promoted by exogenous C5a
735 addition. Adjacent images are representative of DAPT treated rosettes in the presence or absence of
736 C5a. NCAD (white), and computational outlines (green) of rosette apical lumens are shown. L&M)
737 NE-4C cells grown on transwell membranes demonstrate reorganisation of the mitotic spindle (L),
738 as determined by acetylated tubulin staining (green), and reduction in apical surface area (M),
739 outlined by ZO-1 (red) in response to C5a. White arrows are representative distances from mitotic
740 spindle to calculated cell centre as shown in (L). Scale bar = 20 μ m.

741

742 **Fig. 4; C5aR1 signaling alters neural progenitor division planes and proliferation *in vivo*.** A)
743 Schema of the *in utero* injection process. Briefly, 1 μ L 100nM mC5a, 1 μ M PMX53 or vehicle was
744 delivered to the embryonic ventricle *in utero*. After 24 hours, brains were processed for
745 immunohistochemistry. M-phase cells, as determined by pHH₃ staining, were counted along the
746 ventricular surface of the neocortex. B) *In utero* injection of mC5a to the embryonic ventricle
747 increases, whilst blockade of C5aR1 signaling using PMX53 decreases, the number of M-phase
748 apical progenitor cells. C) Cleavage plan analysis demonstrates a shift from symmetric division

749 towards asymmetric division upon treatment with C5aR1 antagonist. S, Symmetric division; A,
750 Asymmetric division; O, Oblique division.

751 **Fig. 5; Blockade of C5aR1 signaling at E12.5-14.5 causes behavioral changes in adult mice. A)**
752 Schema of the experimental process. Briefly, 1mg/kg/day of the C5aR1 antagonist, PMX53, was
753 delivered by intraperitoneal injection to pregnant dams at E12.5-14.5. Resultant litters were taken
754 through behavioral testing from 6-8 weeks, sacrificed and brains prepared for *ex vivo* MRI. Figures
755 display results for vehicle (V, black bars) and PMX53 (P, grey bars) treated mice. B) Sox2/DCX
756 ratio of the ventricular zone of E16.5 embryos. No change in postnatal growth (C), litter size (D),
757 and snout-occiput length (F) was seen. A significant reduction in crown-rump length was observed
758 (E). G) No difference between treatment groups was found in grip strength for both forelimb (F)
759 and hindlimb (H). H) Time to cross balance beam was increased in male animals from PMX53-
760 treated litters. I) Footfall errors crossing balance beam. Distance moved in center of open field
761 arena (J), Frequency of entry to novel arm Y-maze (K), and Time spent immobile during forced
762 swim test (L) were significantly different in PMX53-treated litters.

763

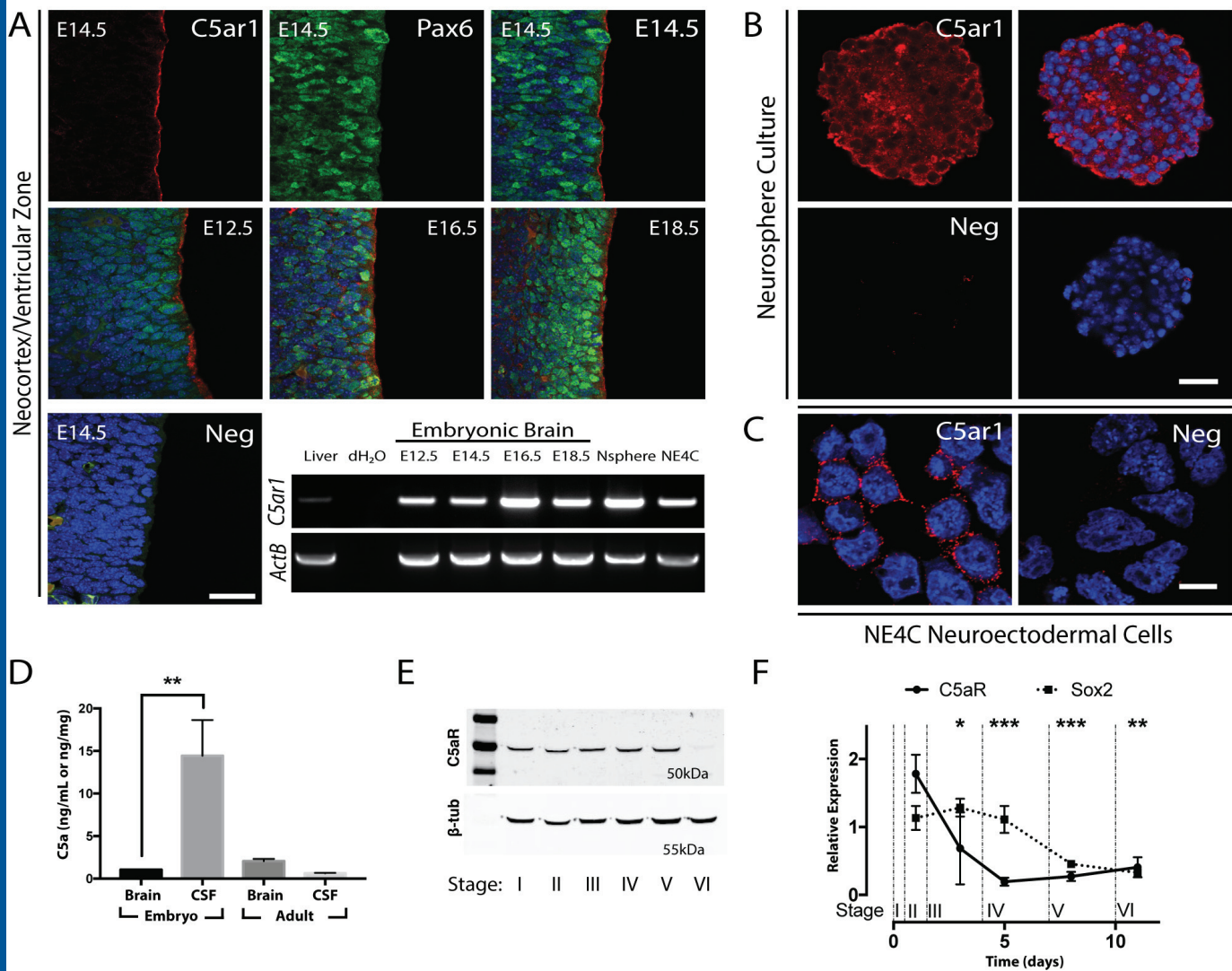
764 **Fig. 6; Blockade of C5aR1 signaling at E12.5-14.5 results in microstructural changes in adult**
765 **brains.** Top row; significance map of jacobian warping projected onto T_1 weighted template
766 average. Middle row; significance map of fractional anisotropy (FA) values projected onto template
767 average. For both maps, vehicle>PMX53 (C5aR1-A) treatment (blue/purple) and PMX53>vehicle
768 (red/yellow). Color coded p-values shown at bottom of figure. Bottom row; Anatomical areas
769 labelled; Mot, motor cortex; Orb, orbital cortex; OB, olfactory bulb; SS, somatosensory cortex;
770 Gust, gustatory cortex; P, piriformis; CP, caudate/putamen; NA, nucleus accumbens; Pal, pallidum;
771 H, hypothalamus.

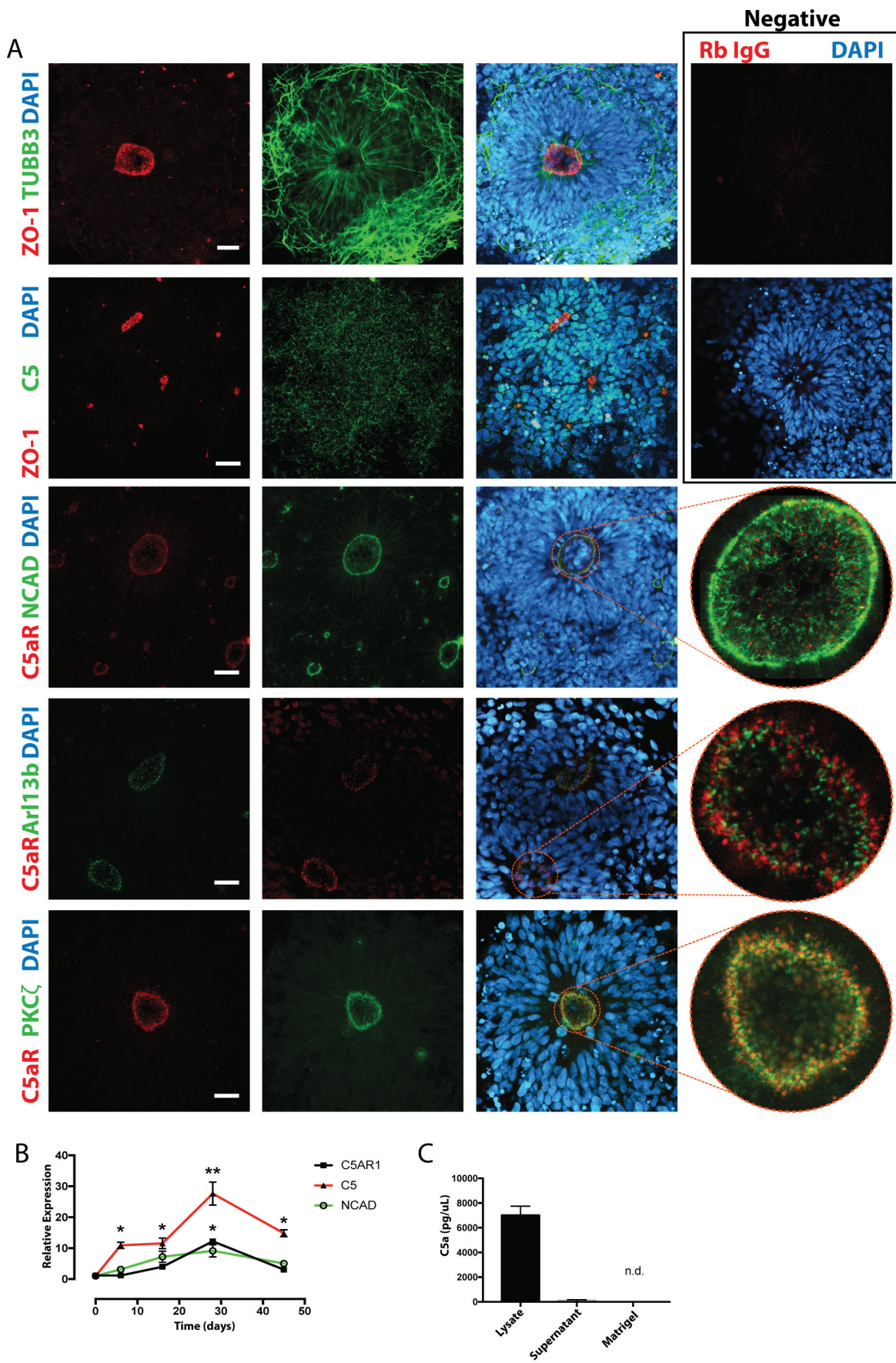
772

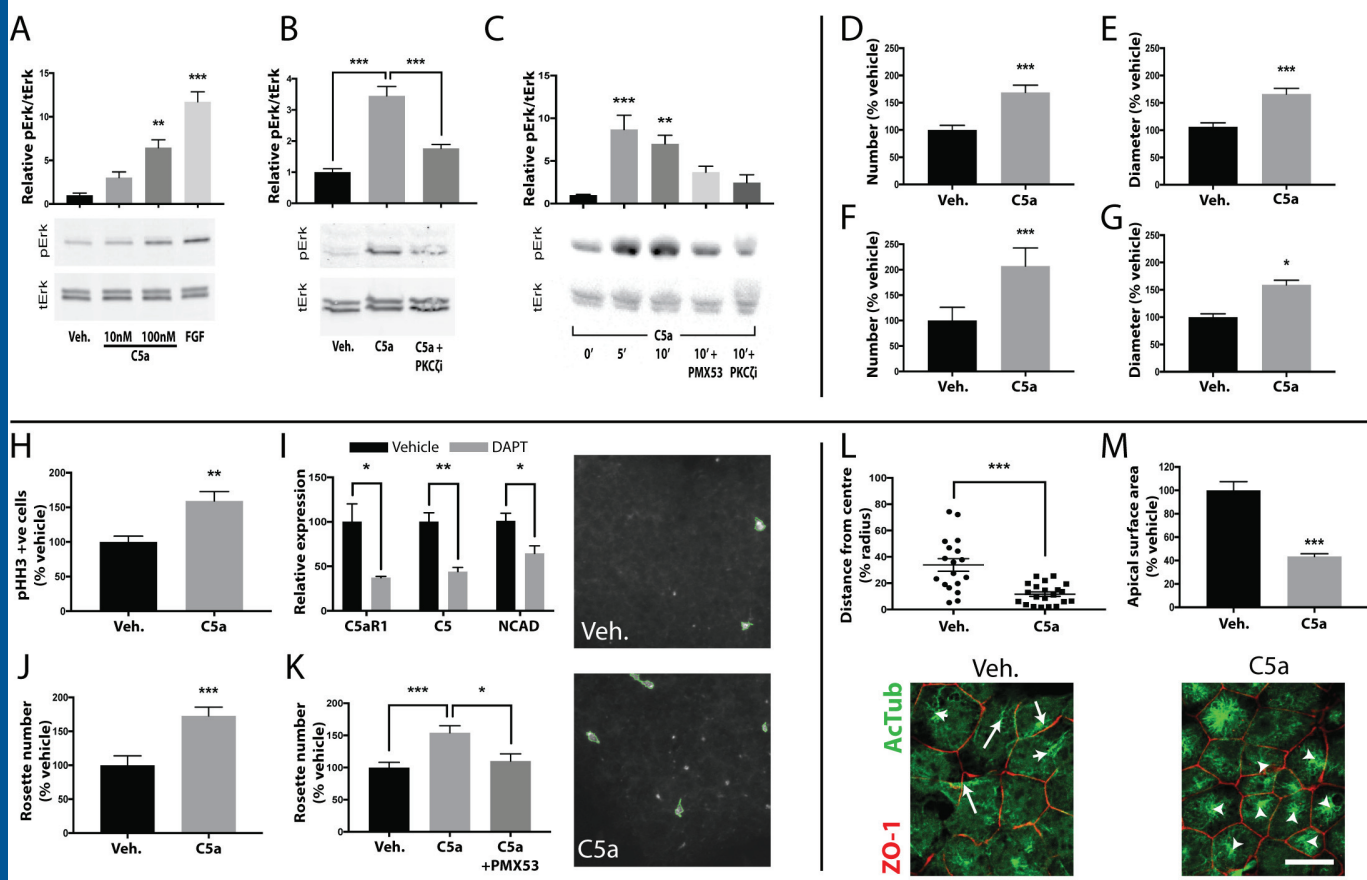
773 **Table 1;** List of PCR primer sequences and conditions.

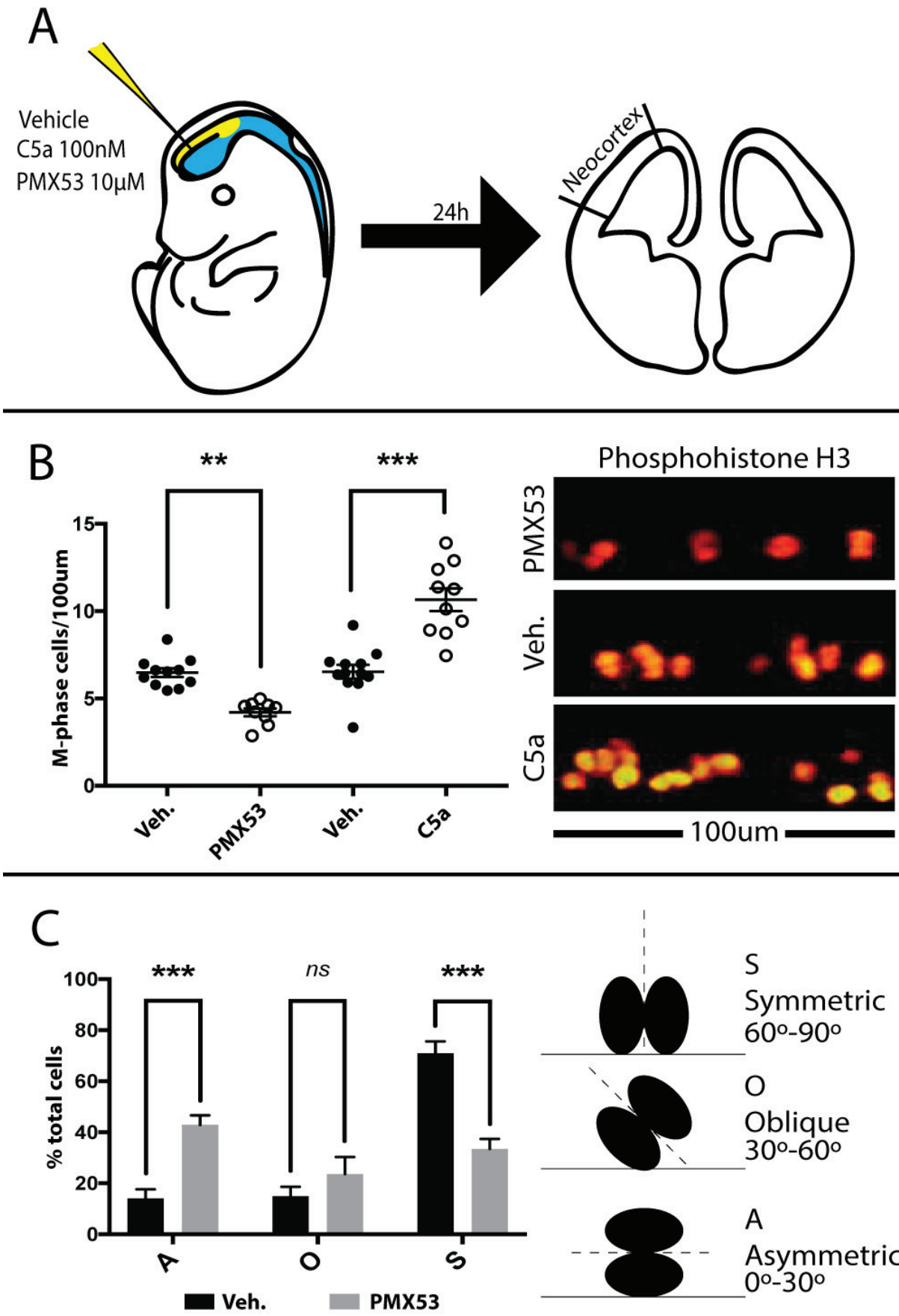
774 **Table 2;** Table of MRI volume comparison of brain regions for C5aR1-antagonist or vehicle treated

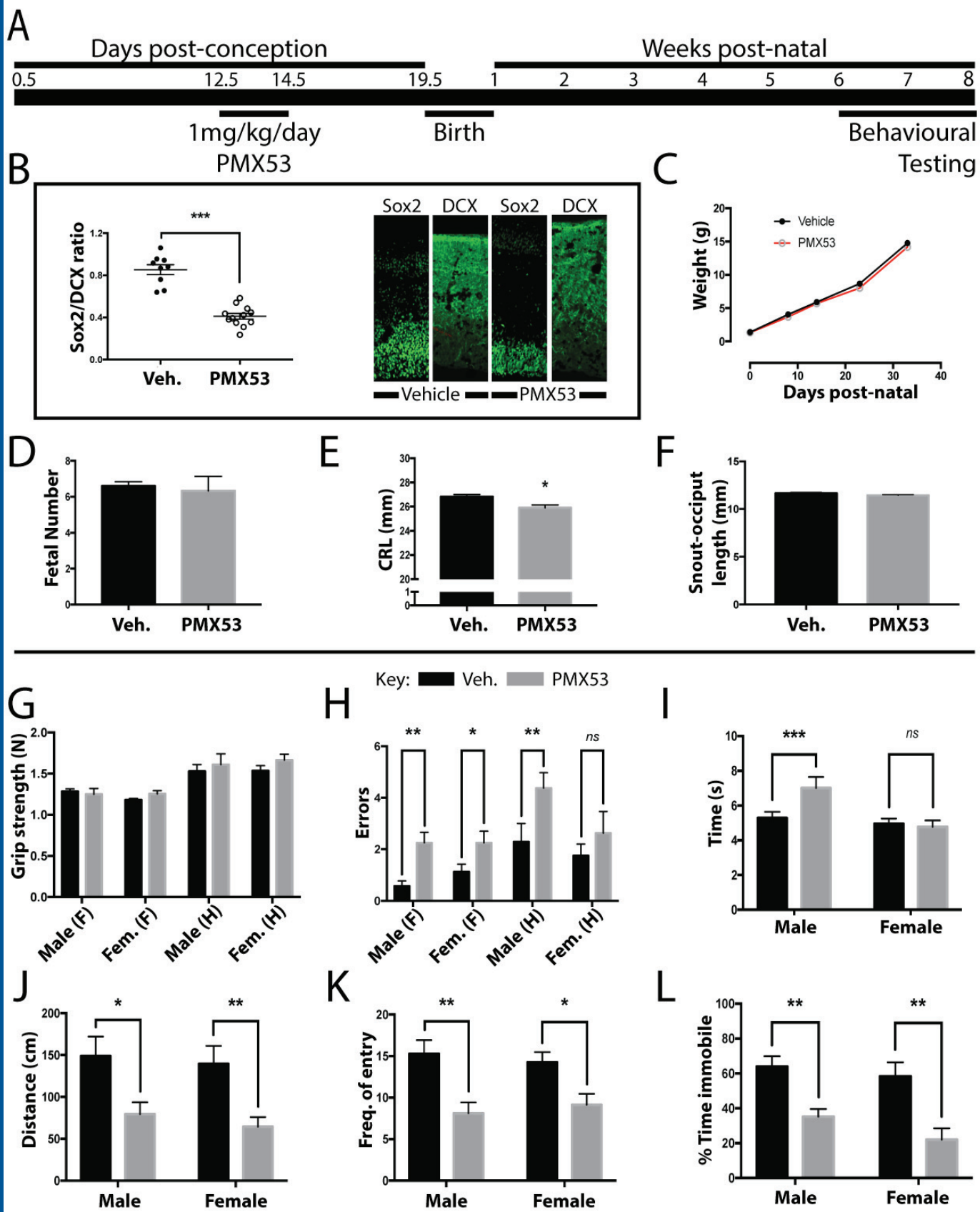
775 mice.

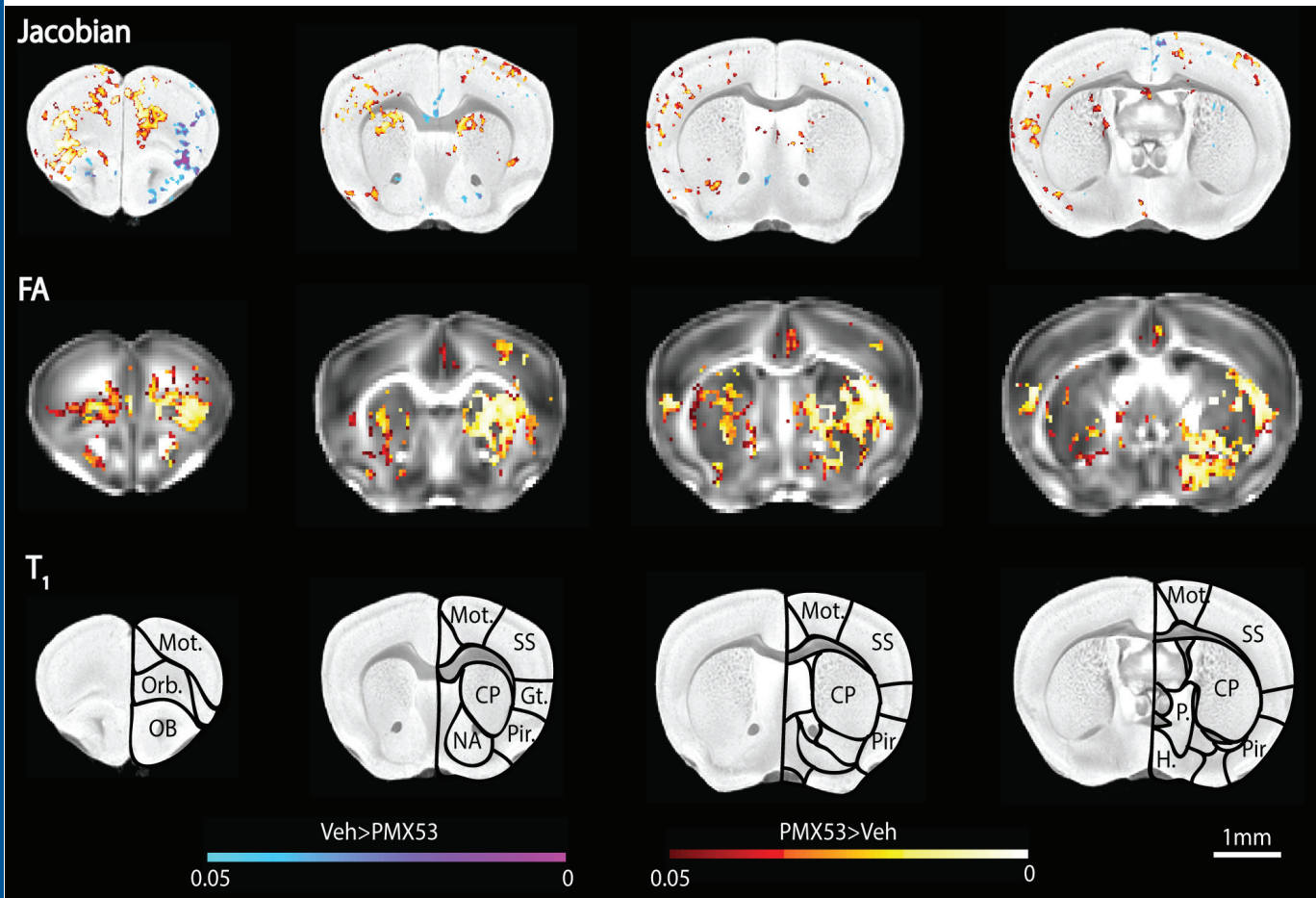












Name	Species	Use	Forward (5'-3')	Reverse (5'-3')	Annealing Temp (°C)	Product size
mC5aR1	Mouse	RT-PCR	ATGCTGATGCTGATGCTGATCG	ATGCTGATGGCTGATCGTCGGATGCTGAT	60	562bp
mActB	Mouse	RT-PCR	GTTGGGCCGCCCTAGGCACCAAG	CTCTTTGATGTCACGCACGATTTC	60	103bp
mC5aR1	Mouse	qPCR	GGGATGTTGCAGCCCTTATCA	CGCCAGATTAGAAACCAGATG	60	131bp
mSox2	Mouse	qPCR	TAGAGCTAGACTCCGGCGATGA	TTTCGTGGTCTTGTAAAGCAA	60	296bp
m18s	Mouse	qPCR	GATCCATTGGAGGGCAAGTCT	CCAAGATCCAACCTACGAGCTT	60	103bp
hC5AR	Human	qPCR	TCCTTCATTATAACCACCCCTGA	GGAAGACGACTGCAAAGATGA	60	139bp
hC5	Human	qPCR	ACTGAATTGGTTGCTACTCCTC	GTATTACTGGACTCCTCCTACC	60	110bp
hACTB	Human	qPCR	CGGGAAATCGTGCCTGACATT	GATGGAGTTGAAGGTAGTTGGTG	60	232bp
hCDH2	Human	qPCR	ATCAACCCCATACACCAGCC	GTCGATTGGTTGACCACGG	60	128bp

Area	Vehicle treatment			C5aR1-A treatment			
	Volume (mm ³)	Std Error	n	Volume (mm ³)	Std Error	n	p value
Amygdala	10.24	0.1425	7	10.18	0.2929	9	0.8764
Caudate/Putamen	23.25	0.4326	7	22.85	0.5933	9	0.6175
CC and External Capsule	8.213	0.102	7	7.891	0.331	9	0.4203
Central Grey Matter	4.476	0.05	7	4.339	0.07	9	0.1762
Cerebellum	46.96	0.3563	7	42.83	1.764	9	0.0624
Fimbria	2.007	0.028	7	1.928	0.05576	9	0.2702
Globus Pallidus	2.485	0.055	7	2.368	0.046	9	0.1209
Hippocampus	24.71	0.287	7	24.31	0.5846	9	0.5832
Hypothalamus	11.61	0.162	7	11.17	0.284	9	0.234
Neocortex	125.5	1.84	7	121.5	3.45	9	0.3668
Olfactory Bulbs	17.88	0.2216	6	16.53	0.7673	9	0.1858
Thalamus	25.19	0.095	7	24.69	0.732	8	0.5444